DAVAO RESEARCH JOURNAL

https://davaoresearchjournal.ph P-ISSN 2244-4432 E-ISSN 2984-7125

# Predicting the unseen: A shoreline shift analysis and prediction along Mayo Bay, Davao Oriental

Fillmore D. Masancay[1]*, Lea A. Jimenez[2]

[1]*Department of Geodetic Engineering, College of Engineering, University of Southeastern Philippines, Davao City, Philippines, Fillmore D. Masancay,ORCID ID: https://orcid.org/0009-0000-9919-7269*
[2]*Regional ICRM Center XI, Davao Oriental State University, Mati City, Davao Oriental, Philippines, Leah A. Jimenez, ORCID ID: https://orcid.org/0009-0005-5170-263X*

Submitted: 30 Sep 2024
Revised: 07 Oct 2024
Accepted: 07 Nov 2024
Published: 04 Dec 2024

**Corresponding author: fdmasancay@usep.edu.ph*

OPEN ACCESS

## ABSTRACT

About 45%-60% of the world's population resides in shoreline areas. Shoreline regions are one of the most vulnerable areas to the effects of global warming. Positions of shorelines are challenging to predict, but the trend of accretion and erosion can be determined using statistical and geospatial techniques. Mati City is a major tourist destination for white sand beaches and pristine waters. Shorelines along Mayo Bay are a source of income for the local community. However, Mayo Bay has been subjected to shifts due to erosion. This study aims to determine the trend of the shoreline shift in Mayo Bay from 2013 to 2023. Landsat 8 OLI satellite images are used in this study. Results reveal that most shorelines experienced erosion, with 97.26% erosion transects. The shoreline length has slightly increased by 0.08% from 2013 to 2023 and is predicted to increase by 3.57% in 2063 and 11.51% by 2100. Barangay Lucatan shows the highest shoreline expansion, while Barangays Bobon and Dahican exhibit the most erosion, with mean rates of -27.15 m/year and -23.60 m/year, respectively. With a classification accuracy of 89% and Root Mean Square Error (RMSE) of 0.05, the study provides a reliable basis for Mayo Bay's shoreline management. The findings will inform erosion mitigation efforts and guide sustainable coastal management plans for at-risk areas.

*Keywords:* Accretion, Digital Shoreline Analysis System (DSAS), Erosion, Geographic Information System (GIS), Remote Sensing

**How to cite:** Masancay, F. D., and Jimenez, L. A. (2024). Predicting the unseen: A shoreline shift analysis and prediction along Mayo Bay, Davao Oriental. *Davao Research Journal*, 15(4), 19-45. https://doi.org/10.59120/drj.v15i4.269

## INTRODUCTION

A shoreline or coastline is a dynamic line connecting water and land (Pajak and Leatherman, 2002; Nandi et al., 2016). Identifying shoreline alterations and their corresponding variability is vital for different coastal studies undertaken by engineers, coastal managers, and coastal scientists (Kankara et al., 2015). The delineation process for shoreline on how much is eroded or accredited through time is difficult due to its dynamic nature (Fenster et al., 2001; Nandi et al., 2016). According to Church and White (2011) and Qiao et al. (2018), the global mean sea level increased from the late 19th century to the beginning of the 21st century by approximately 210 mm and is predicted to grow by the end of the 21st century by 450 mm to 820 mm. Shoreline undergoes long-term and short-term frequent shifts due to geomorphological changes, hydrodynamic changes, and other contributing (Nandi et al., 2016). Mondal (2017) pointed out that the frequent change in shoreline position is duly attributed to anthropogenic activities, tides, waves, and wind. Furthermore, he emphasized erosion as a form of a backward movement of land while accretion is a form of a forward movement caused by these identified natural factors. An updated and accurate information on shoreline change magnitudes will be of huge aid to researchers studying large coastal areas such as safe navigation, aspects of erosion and accretion, designing of defenses for coasts, hazard zoning, environmental protection, sustainable coastal resources management, and predicting future positions of shoreline (Szmytkiewicz et al., 2000; Dellepiane et al., 2004; Maïti and Bhattacharya, 2009; Davidson et al., 2010; Louati et al., 2015). Vulnerable low-lying islands and coastal regions having a huge number of population and substantial infrastructure are susceptible to rising sea levels (Arkema et al., 2013; Johnston et al., 2014; Qiao et al., 2018) and will cause negative impacts on socioeconomic and coastal ecological development (Rahman et al., 2011; Qiao et al., 2018). Boye et al. (2015) state that about 45% to 60% of the global population resides on coasts. Therefore, monitoring regions within the coastal areas is essential for environmental and national development (Rasuly et al., 2010; Qiao et al., 2018).

The Mayo Bay in the City of Mati, Davao Oriental, is geographically located in the southern part of the Philippine Island of Mindanao. The embayment is described as rich in biodiversity, making it one of the most beautiful bays in the world as officiated by the Most Beautiful Bays in the World Association, as reported by SunStar Davao (2020). The study aims to analyze the short-term and predict the long-term shoreline trend in Mayo Bay, Davao Oriental. Short-term analysis is based on the rate of shifts from 2013 (baseline year) to 2023, while long-term analysis is after 50 years (2063) and at the end of the century (2100). The study focuses on the following research gaps: insufficiency of local shoreline shift-related studies, lack of modern techniques and technical experts in monitoring shorelines and detecting shifts, and coastal management-related gaps. It is very challenging to search for local studies. Currently, there are no research studies on the monitoring and detecting shoreline shifts along the Davao Region. Most research studies focused on marine ecosystems and none on the short-term and long-term shift detection along these shorelines. There is also an insufficiency in integrating Geographic Information Systems (GIS) and Remote Sensing (RS) in studying shorelines, especially in the Davao Region. The researcher utilizes internationally published research studies focusing on shoreline shift detection and applies those concepts, principles, and findings in Mayo Bay. If published, this will be the first research study to focus on shoreline shifts in Mayo Bay and will also serve as a baseline for further relevant studies. Modern techniques and technical experts are lacking in monitoring shoreline shifts. This research highlights the significance of integrating GIS and RS as a cost-effective and reliable tool for monitoring shoreline shifts. There is a limitation in the

 DOI: https://doi.org/10.59120/drj.v15i4.269

availability of historical shoreline data, which will aid in analyzing shoreline shift trends. Free/Open-source satellite images are used in this study. Despite the limitations, RS techniques such as geometric correction, radiometric correction, accuracy assessment, and root mean square error (RMSE) are applied to produce a holistic model. There is a lack of user-friendly platforms for various stakeholders to detect shoreline shifts. Advanced techniques in RS are needed to obtain high accuracy in determining shoreline shifts, especially in changing environmental conditions. The researcher chose Mayo Bay as the study area since the agencies managing the shoreline areas of Mayo Bay are crafting an integrated coastal management (ICM) policy to comprehensively strengthen the implementation, protection, and management of shorelines. GIS and RS provide satellite image analysis, allowing comprehensive assessments of the shorelines over time. By identifying the eroding and accreting areas, the concerned agencies can prioritize vulnerable areas through various governmental interventions. Overall, it will support coastal policymakers in understanding the shoreline shift trend along Mayo Bay and help them implement the appropriate management strategies.

## MATERIALS AND METHODS

### Study area

Mayo Bay is geographically located on the southern part of the Philippine Island of Mindanao at 6.79O – 7O N latitude and 126.31O– 126.41O E longitude (Figure 1). It is adjacent to Pujada Bay and is located between the two (2) headlands, Tarragona in the east and Guang-Guang Peninsula in the west. It is rich in biodiversity. It is a nest of marine turtles (e.g., Chelonia mydas, Eretmochelys imbricata, Lepidochelys olivacea, and Dermochelys coriacea) (Jimenez and Inabiogan, 2019b) and dugong (Jimenez and

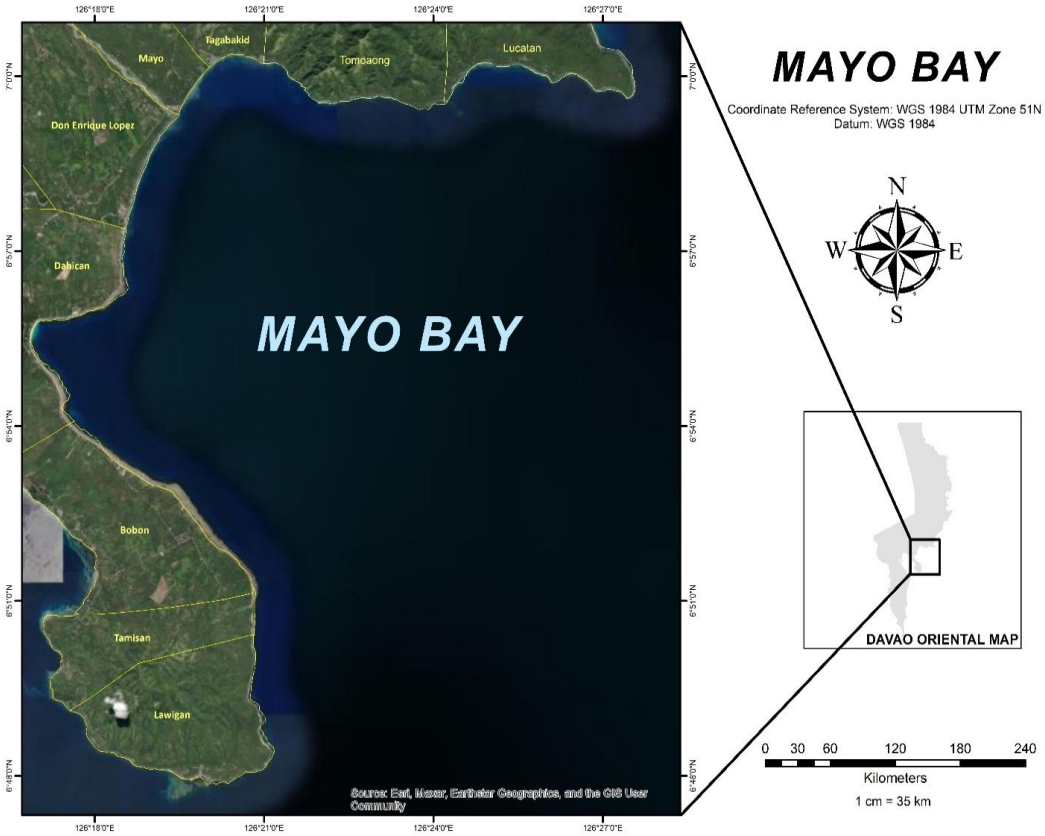


**Figure 1.** Map of the study area showing the coastal barangays surrounding Mayo Bay (Source: Esri, Maxar, Earthstar Geographics, and the GIS User Community).

Inabiogan, 2019a). The Bay serves as the catchment of runoffs from the terrestrial side, rivers, watersheds, and smaller tributaries in Barangays Lucatan, Bobon, Mayo, Tagabakid, and Dahican (National Mapping and Resource Information [NAMRIA], 2015) drain into the Bay which provides freshwater input and nutrients. The Bay is a mixture of Pacific waters exchanged through the surrounding catchment areas and tidal fluctuations that carry their respective physiochemical signatures. Global oceanic processes occur on this side of the Pacific Ocean and have significant roles in global climatologies, such as the Mindanao current. Mindanao current is generated by the North Equatorial Current bifurcation adjacent to the Philippine coast. Mindanao flows south of the Philippine Sea along the Mindanao Coast, enabling fresh water and heat exchange to the Indian and the North Pacific Ocean (Schonau et al., 2015). Schonau (2015) further elucidated that the transport process of the Mindanao Current influences the available nutrients, marine ecosystem productivity, and various climate phenomena such as the El Niño Southern Oscillation.

**Sources of data**

In this study, multi-temporal satellite data from Landsat 8 OLI from year 2013 and 2023 are employed. However, the insufficient satellite imagery with less clouds during the selected period prevents the satellite images from being taken at regular intervals. Acquired satellite images have a cloud cover of 15% or less. Landsat 8 OLI satellite image data are accessed from https://earthexplorer.usgs.gov/. Landsat 8 carries the operational land imager (OLI) and the thermal infrared sensor (TIRS) instruments. OLI measures the visible, near-infrared, and short-wave infrared portions of the spectrum. Landsat 8 satellite images have a 30-meter multi-spectral spatial resolution and 15-meter panchromatic along a 185-kilometer swath. Landsat 8 orbits the Earth in a sun-synchronous, near-polar orbit at 705 km altitude. It completes one Earth orbit every 99 minutes and has a 16-day repeat cycle with an equatorial crossing at 10:00 a.m. It acquires about 750 scenes daily on the World Reference System-2 (WRS-2) path/row system with a swath overlap varying from 7 percent at the equator to a maximum of 85 percent approximately at extreme latitudes. Landsat 8 OLI contains nine (9) spectral bands: band 1 coastal aerosol (0.43 - 0.45 µm), band two blue (0.450 - 0.51 µm), band three green (0.53 - 0.59 µm) 30 m, band four red (0.64 - 0.67 µm), band five near-infrared (0.85 - 0.88 µm), band six short wave infrared (SWIR) (1.57 - 1.65 µm), band 7 SWIR 2 (2.11 - 2.29 µm), band eight panchromatic (0.50 - 0.68 µm), and band nine cirrus (1.36 - 1.38 µm) (USGS, 2024).

**Data analysis**

The Digital Shoreline Analysis System (DSAS) software is utilized to analyze and identify the erosion-accretion portions along the shorelines of Mayo Bay. It measures the change in shoreline by comparing the position of both shorelines. A transect line will determine the extent of shifting, which also serves as a tool for prediction. Utilizing DSAS software, which seamlessly integrates with GIS, variations along the shoreline are discovered following shoreline extraction. It calculates the rate of shift statistics for a time series of vector data related to shorelines. Transects that are cast perpendicular to the baseline are generated for this purpose by DSAS. In this study, a 100-meter interval per transect is used. The rate of shift statistics is then computed using the transect shoreline intersections along this baseline. Based on the DSAS methodology, the shoreline rate of shift is calculated using two different statistical techniques: First is the identification of the distance between the oldest and newest shorelines for each transect, and second is the division of the distance between the oldest and latest shoreline movement by the amount of time that has passed between them and the EPR is calculated with unit in meter per year. Positive values demonstrate accretion along the shoreline, while negative values obtained using this methodology represent erosion.


DOI: https://doi.org/10.59120/drj.v15i4.269

The study is limited to identifying a decade of shoreline shift along Mayo Bay (2013 to 2023) using Landsat 8 OLI satellite imagery with a resolution of 30 meters. Satellite images from 2013 to 2023 with 15% or less cloud cover are chosen for erosion-accretion change. Accuracy assessment and the RMSE are applied to the generated maps to address the limitations in the resolution of the satellite imagery used. DSAS automatically chose transects along the shoreline following the 100 m interval for the shoreline erosion-accretion coverage.

## The procedure of the study

Figure 2 presents the study's methodological framework, showcasing the data collection processes.

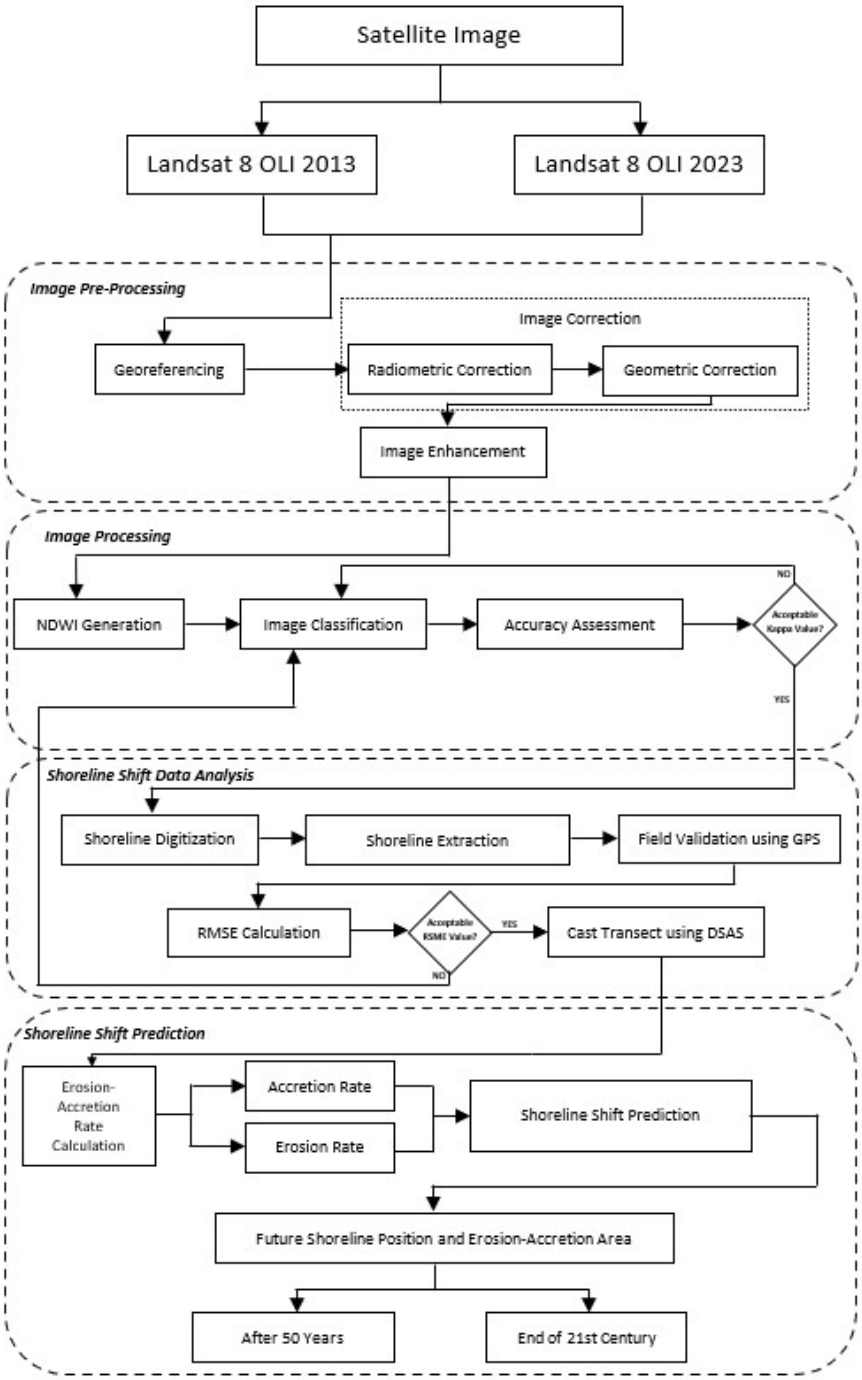


**Figure 2.** The methodological framework of the study.

**Image Pre-Processing**

The Landsat 8 OLI satellite images for 2013 and 2023 undergo necessary preparations. This will ensure the accuracy of the satellite images utilized in the study. Downloaded Landsat 8 OLI satellite images are added to GIS software as raster files. Shapefiles for the boundary of Mati City and Tarragona municipality are imported as they serve as the spatial data boundary.

**Georeferencing**

Satellite images first undergo georeferencing. The United States Geological Survey (USGS) defines georeferencing as an internal coordinate system relating a ground system of geographic coordinates to an aerial photo or a digital map where every point on the map has a corresponding location on the surface of the Earth (USGS, 2024). The satellite images undergo aligning of satellite images points to their corresponding geographic coordinates on the ground. Conducting georeferencing is crucial as it allows accurate analysis of spatial data.

**Image correction**

Georeferenced satellite images undergo image correction. The most commonly used image correction is the geometric and radiometric correction.

**Geometric correction**

Geometric correction is conducted to eliminate the geometric anomalies and develop a representation of the original scene by means of pixel location errors correction and the establishment of the incorrect position and ground attributes coincidence in the image (Olmanson et al., 2001).

**Radiometric correction**

Radiometric correction uses dark object subtraction which reduces the influence of the atmosphere in the satellite images as these reduces the quality of the satellite images. The lowest value of the pixel in an image is assumed to be equal to zero (Natih et al., 2020).

**Image processing**

Normalized Difference Water Index (NDWI) generation

Enhanced satellite images are subjected to NDWI generation. NDWI helps identify the open water features and highlights them against vegetation and soil on a satellite image (Sryberko, 2023). Figure 3 shows the 2013 and 2023 NDWI maps. According to Elnabwy et al. (2020), NDWI provides an excellent demarcation of the coastline along with the red, green, and blue (RGB) system. NDWI is obtained by utilizing near-infrared and green band combinations of satellite image data, allowing it to detect changes in water bodies. Green represents band 3, while the near-infrared represents band 5. McFeeters, in 1996, proposed that it detect and monitor slight alterations in the water content of water bodies. NDWI is capable of highlighting water bodies in a satellite image using enhancement. To calculate NDWI for Landsat 8 OLI, use the equation written as:

$$NDWI = \frac{(Green - Near\text{-}infrared(NIR)}{(Green + Near\text{-}infrared(NIR)}$$

The visible green wavelengths optimize the reflectance of the surface of water. The near-infrared wavelength optimizes the high reflectance of the terrestrial vegetation and soil features while the low reflectance of water features is minimized. The result for the NDWI equation is a negative value or zero for land features and positive values for water features.


DOI: https://doi.org/10.59120/drj.v15i4.269

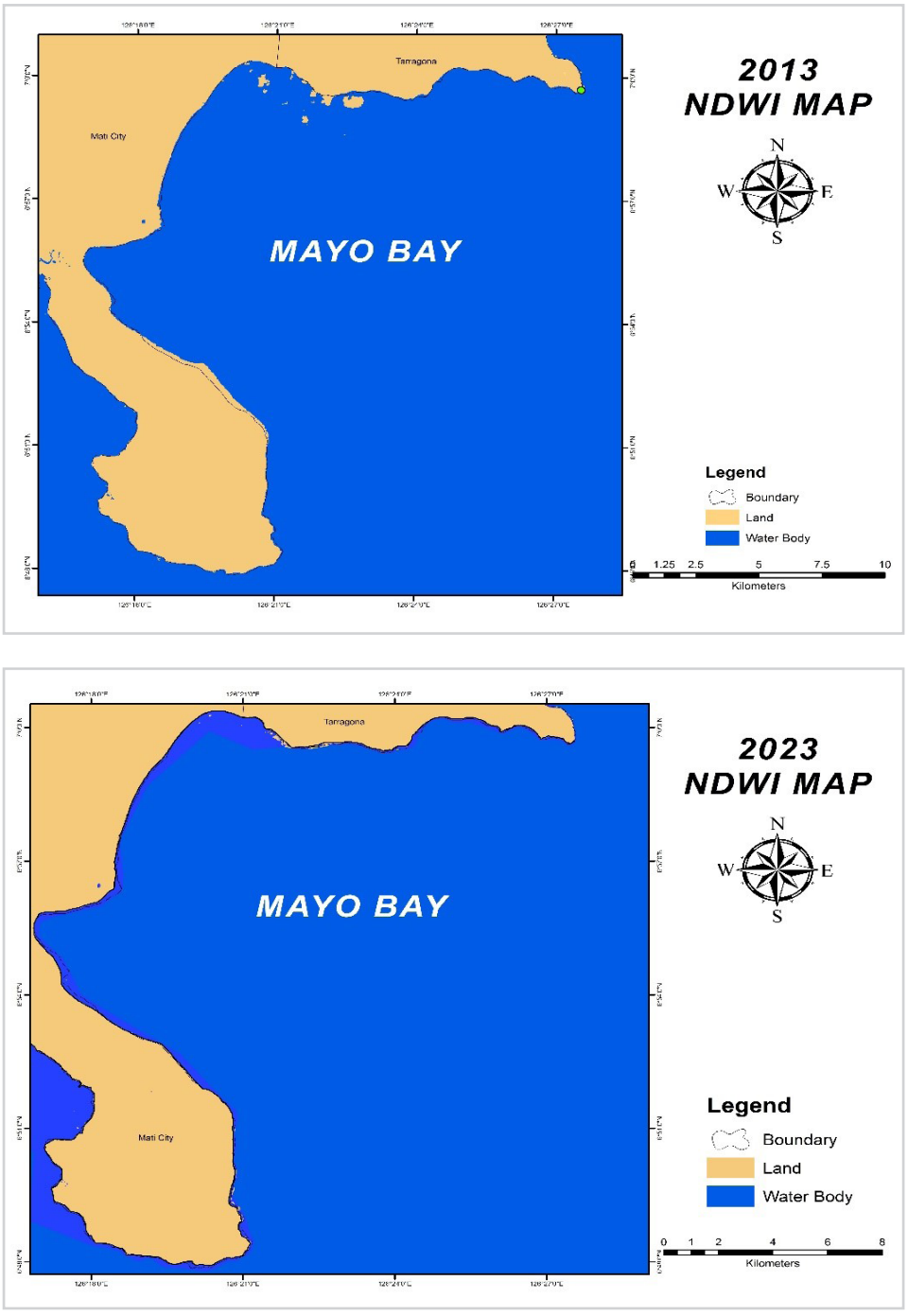


**Figure 3.** 2013 and 2023 NDWI Map.

## Image classification

After generating NDWI, the satellite images undergo image classification. Image classification of shorelines is necessary as it improves the accuracy of the extracted shoreline change (Lu and Weng, 2007). This helps in grouping pixels of the same class. In this case, the study area is divided into two (2) classes only as the study will focus on identifying the shoreline of the line separating the land and water areas along Mayo Bay. The blue color is used to represent the water body, and brown is used to describe the land area.

**Accuracy assessment**

A classified image is assessed to test its accuracy. Elnabwy et al. (2020) stress that accuracy assessment or validation is essential in RS data processing. Accuracy assessment parameters are beneficial for model performance assessment of a specific class or category of a particular study interest. Image classification accuracy is commonly measured using a confusion/error matrix. Rwanga and Ndambuki (2017) define a confusion matrix as a simple cross-tabulation sample set of reference data in the ground and the mapped class label. In this study, the overall accuracy and Kappa statistics are used to assess the accuracy of the classified satellite images.

The overall accuracy can be acquired using this formula:

$$\text{Overall Accuracy} = \frac{\text{n (total number of corrected pixel)}}{\text{N (total numbe of pixel of raw image)}}$$

Kappa analysis is a discrete multivariate technique utilized for image classification accuracy assessment and measurement of agreement between the reference data and classified map (Elnabwy et al., 2020). Kappa statistics range from 0 to 1, representing the highest agreements by values closest to 1. Kappa statistics is calculated using this formula (Jenness and Wynne, 2007):

$$\text{Kappa Coefficient} = \frac{N \sum_{i=1}^{r} Xii - \sum_{i=1}^{r} (Xi+ * X+i)}{N2 - \sum_{i=1}^{r} (Xi+ * X+i)}$$

Where: N is the total number of observations (pixels), $r$ is the number of columns and rows in the error matrix, $X+i$ is the marginal total of column $i$, $Xi+$ is the marginal total of row $i$, and $Xii$ is the observation in column $i$ and row $i$.

Table 1 shows the kappa statistics rating criteria reproduced by Rwanga and Ndambuki (2017) based on the categorization by Landis and Koch (1977), which is widely referenced. Kappa statistics less than 0 represent poor agreement. Kappa statistics equal to 0 to 0.20 represents slight agreement. Kappa statistics equal to 0.21 to 0.40 represents fair agreement. Kappa statistics equal to 0.41 to 0.60 indicates moderate agreement. Kappa statistics equal to 0.61 to 0.80 indicates substantial agreement. Kappa statistics equal to 0.81 to 1.00 shows almost perfect agreement.

**Table 1.** Kappa statistics rating criteria by Rwanga and Ndambuki (2017).

| Kappa statistics | Strength of agreement |
|---|---|
| <0.00 | Poor |
| 0.00-0.20 | Slight |
| 0.21-0.40 | Fair |
| 0.41-0.60 | Moderate |
| 0.61-0.80 | Substantial |
| 0.81-1.00 | Amost perfect |


DOI: https://doi.org/10.59120/drj.v15i4.269

**Shoreline shift data analysis**
**shoreline digitization**

Satellite images with an acceptable accuracy value are then subjected to shoreline digitization. The digitized satellite image is subjected to image reclassification. The satellite image, which is in raster format, is converted to polygon. Shorelines are then digitized by tracing the polygon within the satellite image, which is saved in vector format or shapefiles.

**Shoreline extraction**

Shoreline extraction is conducted after shoreline digitization. Maiti and Bhattacharya (2009) state that a saturated zone at the water-land boundary makes automatic shoreline delineation complex.

**Field validation**

The researcher uses the Garmin ETREX 221X Global Positioning System (GPS) device to conduct field validation along the coastal barangays surrounding Mayo Bay. The Garmin ETREX 221X GPS is a handheld dual-satellite measurement positioning navigator. It is a suitable device to be utilized for ground truthing as it enhances the possibility of receiving two (2) satellite systems at the same time. The Root Mean Square Error (RMSE) is used to validate the generated model in this study. RMSE is determined to validate, compare, and estimate the model output error from the predicted and actual location of the shoreline. (Nandi et al., 2016). RMSE can be calculated using this equation:

$$RMSE= \sqrt{(XMod-XOrg)^2 - (YMod-YOrg)^2}$$

Where XMod and YMod represents the generated coordinates of the model X and Y of the shoreline while XOrg and YOrg represents the actual coordinates of X and Y of the shoreline. The resulting RMSE value will be evaluated according to its performance to test the model's accuracy. Table 2 shows the RMSE ranges and the corresponding performance.

**Table 2:** RMSE ranges for model performance (Oke et al., 2020).

| Root Mean Square Error (RSME) range | Performance |
|---|---|
| < 0.009 | Excellent prediction accuracy |
| 0.009 < RMSE < 0.09 | Good prediction accuracy |
| 0.09 < RMSE < 0.5 | Reasonable prediction |
| >0.5 | Inaccurate prediction |

**Cast transect from baseline**

Transects from the baseline method are considered and utilized by the Federal Emergency Management Agency (FEMA) as a standard method for determining long-term coastal hazard zones and coastal change rates vulnerable to severe erosion (Crowell et al., 1991). Casting of Transect with the aid of DSAS software. Nandi et al. (2016) point out that transects from the baseline approach are based mainly on a statistical approach. A personal geo-database is then created where the shapefiles for the 2013 and 2013 shorelines are stored following the same coordinate system as the satellite image. Feature classes for 2013 and 2023 shorelines are created. 2023 shoreline

is stored as a line feature type in the feature class with field names (OBJECTID, SHAPE, SHAPE_Length, DATE_, and UNCERTAINTY) and its corresponding data type (Object ID, Geometry, Double, Text, and Double). 2013 shoreline is stored as a line feature type in the feature class with field names (OBJECTID, SHAPE, SHAPE_Length, ID, and GROUP_) and its corresponding data type (Object ID, Geometry, Double, Long Integer, and Long Integer). Create a buffer that serves as the basis for establishing the baseline. Transects are cast. Erosion and accretion rates of points identified by the transects or the straight line intersecting the shoreline are then determined.

**Erosion-Accretion rates calculation**

Shoreline shift rates are calculated using a confidence level of 95%. The erosion and accretion rates are generated using the End Point Area (EPR) method. The shoreline shift data generated by DSAS software presents the erosion and accretion rates of the different portions of the shoreline as identified by the casted transects.

**Shoreline shift prediction**

The EPR prediction model is used in this study as it is the most commonly used shoreline shift prediction model by coastal managers in forecasting future erosion and accretion rates of a particular location due to its simplicity. Data are presented in meter/s per year unit. Positive values mean accretion, while negative values mean erosion. EPR is the most commonly used method for determining the rate of change and prediction of the future position of the shoreline. It is widely used, especially by coastal land managers and planners, and has become popular due to its robustness and simplicity (Li et al., 2001; Nandi et al., 2016). Moreover, Nandi et al. (2016) also point out that the EPR method is computed using the latest position and a baseline. Any information relevant to the shoreline, such as tidal information, sea current data, sediment supply, sea wave, etc., is not required for analysis because it is only anchored on the historical and recent shoreline map. The total rate of change on shoreline distance is divided by the difference in the elapsed time. It only solves shoreline shift rates with two (2) different dates and is calculated for different combinations for more than two shorelines (Ciritci and Türk, 2019). ERR method is a major advantage for shoreline shift prediction since any shoreline-related information, such as sea current data, tidal information, sediment supply, sea wave data, etc., are not required for the analysis since it is based on the historical and most recent shoreline map (Nandi et al., 2016).

**RESULTS**

**Accuracy assessment**

Table 3 shows the error matrix of the satellite image for 2013 for accuracy assessment. There are 5 classes used for assessing the accuracy of the satellite image: water body, built-up, land, agricultural land, and forest. There is a total of 100 accuracy assessment points. Out of the 34 total water body accuracy assessment points in the reference data and 35 total water body accuracy assessment points in the classified data, 32 accuracy assessment points are classified as water bodies. Of the 18 total built-up accuracy assessment points in the reference data and 17 total built-up accuracy assessment points in the classified data, 15 are classified as built-up. Out of the 24 total land accuracy assessment points in the reference data and 28 total land accuracy assessment points in the classified data, 24 accuracy assessment points are classified as land. Out of the 17 total agricultural land accuracy assessment points in the reference data and 15 total agricultural land accuracy assessment points in the classified data, 13 accuracy assessment points are classified as agricultural land. Out of the 7 total forest accuracy assessment points in the reference data and 5 total forest accuracy assessment points in the classified data, 5 accuracy assessment points are classified as forest.


DOI: https://doi.org/10.59120/drj.v15i4.269

**Table 3.** Error matrix for 2013 satellite image.

| | | Reference data | | | | | |
|---|---|---|---|---|---|---|---|
| | **Class value** | **Waterbody** | **Built-up** | **Land** | **Agricultural land** | **Forest** | **Total** |
| Classified data | Waterbody | 32 | 1 | 0 | 2 | 0 | 35 |
| | Built-up | 2 | 15 | 0 | 0 | 0 | 17 |
| | Land | 0 | 0 | 24 | 2 | 2 | 28 |
| | Agricultural land | 0 | 2 | 0 | 13 | 0 | 15 |
| | Forest | 0 | 0 | 0 | 0 | 5 | 5 |
| | Total | 34 | 18 | 24 | 17 | 7 | 100 |

Table 4 shows the error matrix of the satellite image for 2023 for accuracy assessment. There are 5 classes used for assessing the accuracy of the satellite image: water body, built-up, land, agricultural land, and forest. There are a total of 100 accuracy assessment points. Out of the 28 total water body accuracy assessment points in the reference data and 31 total water body accuracy assessment points in the classified data, 27 accuracy assessment points are classified as water bodies. Of the 19 total built-up accuracy assessment points in the reference data and 20 total built-up accuracy assessment points in the classified data, 17 are classified as built-up. Out of the 26 total land accuracy assessment points in the reference data and 25 total land accuracy assessment points in the classified data, 24 accuracy assessment points are classified as land. Out of the 13 total agricultural land accuracy assessment points in the reference data and 11 total agricultural land accuracy assessment points in the classified data, 10 accuracy assessment points are classified as agricultural land. Out of the 14 total forest accuracy assessment points in the reference data and 13 total forest accuracy assessment points in the classified data, 12 accuracy assessment points are classified as forest.

**Table 4.** Error matrix for 2023 satellite image.

| | | Reference data | | | | | |
|---|---|---|---|---|---|---|---|
| | **Class value** | **Waterbody** | **Built-up** | **Land** | **Agricultural land** | **Forest** | **Total** |
| Classified data | Waterbody | 27 | 1 | 1 | 1 | 1 | 31 |
| | Built-up | 0 | 17 | 1 | 1 | 1 | 20 |
| | Land | 0 | 1 | 24 | 0 | 0 | 25 |
| | Agricultural land | 1 | 0 | 0 | 10 | 0 | 11 |
| | Forest | 0 | 0 | 0 | 1 | 12 | 13 |
| | Total | 28 | 19 | 26 | 13 | 14 | 100 |

**Field validation**

Table 5 shows the predicted and actual geographic coordinates in latitudes and longitudes of the ground control points (GCP) in this study as part of ground truthing. 11 GCPs were used and spread all over the study area. The researcher used a GPS device to gather the actual geographic coordinates of each GCP. These points are used to determine the RMSE value of the generated maps. Figure 6 shows the location of the GCPs used in field validation.

**Table 5.** Predicted and actual coordinates of Ground Control Points (GCP).

| Ground Contro Points (GCP) | Barangay | Predicted latitude | Actual latitude | Predicted longitude | Actual longitude |
|---|---|---|---|---|---|
| 1 | Don Enrique Lopez | 6.959953 | 6.960130556 | 126.308995 | 126.3089833 |
| 2 | Dahican | 6.929966 | 6.930297222 | 126.259887 | 126.2599528 |
| 3 | Dahican | 6.928975 | 6.929308333 | 126.272992 | 126.27295 |
| 4 | Dahican | 6.932533 | 6.9325 | 126.25531 | 126.2553444 |
| 5 | Dahican | 6.943612 | 6.943541667 | 126.246689 | 126.2466611 |
| 6 | Dahican | 6.952221 | 6.952255556 | 126.217207 | 126.2172306 |
| 7 | Mayo | 6.800655 | 6.991522 | 126.452976 | 126.325238 |
| 8 | Tagabakid | 7.101389 | 7.004427 | 126.309002 | 126.335797 |
| 9 | Bobon | 6.8572912 | 6.877162 | 126.400219 | 126.326344 |
| 10 | Tamisan | 6.8391768 | 6.842269 | 126.2908705 | 126.346404 |
| 11 | Lawigan | 6.8907801 | 6.837113 | 126.237703 | 126.346367 |

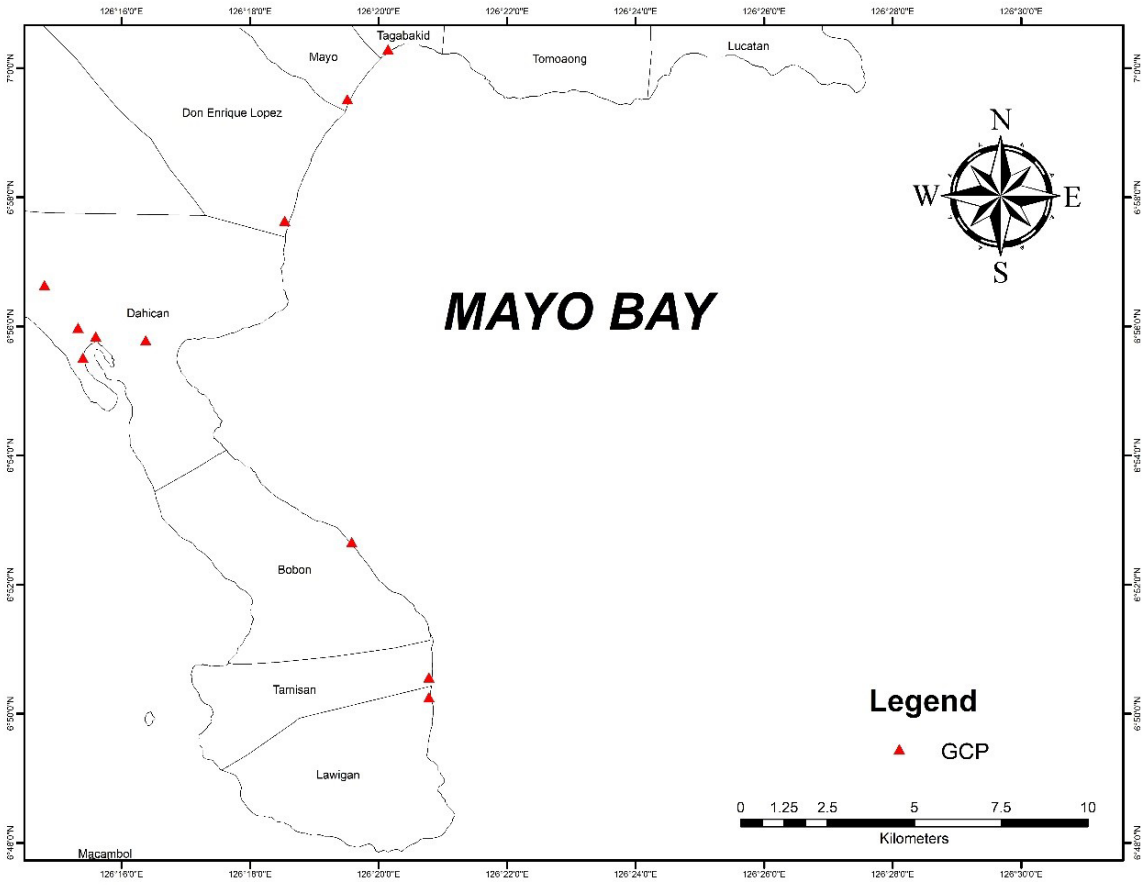


**Figure 4.** Map showing location of the Ground Control Points (GCP) used in field validation.

**Shoreline shift**

Table 6 shows the number of erosion and accretion transects per barangay in Mayo Bay. There are a total of 474 transects, 461of which are erosion transects, while 13 are accretion transects.


DOI: https://doi.org/10.59120/drj.v15i4.269

**Table 6.** Number of erosion and accretion transects.

| Barangay | Erosion | Accretion |
|---|---|---|
| Lucatan | 73 | 0 |
| Tomoaong | 62 | 6 |
| Tagabakid | 13 | 3 |
| Mayo | 16 | 1 |
| Don Enrique Lopez | 37 | 0 |
| Dahican | 92 | 2 |
| Bobon | 86 | 0 |
| Tamisan | 17 | 1 |
| Lawigan | 65 | 0 |
| Total | 461 | 13 |

Barangay Lucatan has a total of 73 erosion transects and no accretion transect. Barangay Tomoaong has a total of 62 erosion transects and 6 accretion transects. Barangay Tagabakid has a total of 13 erosion transects and 3 accretion transects. Barangay Mayo has a total of 16 erosion transects and one accretion transect. Barangay Don Enrique Lopez has 37 erosion transects and no accretion transect. Barangay Dahican has a total of 92 erosion transects and 2 accretion transects. Barangay Bobon has a total of 86 erosion transects and no accretion transect. Barangay Tamisan has a total of 17 erosion transects and 1 accretion transect. Barangay Lawigan has a total of 65 erosion transects and no accretion transect.

**Table 7.** Mean erosion, accretion, and total shift rate in m/yr.

| Barangay | Mean erosion rate (m/yr) | Mean accretion rate (m/yr) |
|---|---|---|
| Lucatan | -3.30 | 0.00 |
| Tomoaong | -3.24 | 2.61 |
| Tagabakid | -2.16 | 0.13 |
| Mayo | -2.53 | 3.15 |
| Don Enrique Lopez | -2.96 | 0.00 |
| Dahican | -9.57 | 2.14 |
| Bobon | -16.42 | 0.00 |
| Tamisan | -6.47 | 0.29 |
| Lawigan | -4.03 | 0.00 |

Table 7 shows the mean erosion and accretion rate per barangay in Mayo Bay. Barangay Lucatan has a mean erosion rate of -3.30 m/yr. Barangay Tomoaong has a mean erosion rate and an accretion rate of -3.24 m/yr and +2.61 m/yr. Barangay Tagabakid has a mean erosion rate of -2.16 m/yr and an accretion rate of +0.13 m/yr. Barangay Mayo has a mean erosion rate of -2.53 m/yr and an accretion rate of +3.15 m/yr. Barangay Don Enrique Lopez has a mean erosion rate of -2.96 m/yr. Barangay Dahican has a mean erosion rate of -9.57 m/yr and an accretion rate of +2.14 m/yr. Barangay Bobon has a mean erosion rate of -16.42 m/yr. Barangay Tamisan has a mean erosion rate of -6.47 m/yr and an accretion rate of +0.29 m/yr. Barangay Lawigan has a mean erosion rate of -4.03 m/yr.

**Table 8.** Maximum and minimum erosion and accretion rate.

| Barangay | Erosion rate (m/yr) | | Accretion rate (m/yr) | |
|---|---|---|---|---|
| | Maximum | Minimum | Maximum | Minimum |
| Lucatan | -7.71 | -0.29 | 0.00 | 0.00 |
| Tomoaong | -8.93 | -0.14 | 4.49 | 1.51 |
| Tagabakid | -3.27 | -0.08 | 0.29 | 0.11 |
| Mayo | -3.84 | -0.53 | 3.15 | 3.15 |
| Don Enrique Lopez | -6.04 | -0.56 | 0.00 | 0.00 |
| Dahican | -23.60 | -1.88 | 2.25 | 2.02 |
| Bobon | -27.15 | -7.83 | 0.00 | 0.00 |
| Tamisan | -13.54 | -0.40 | 0.29 | 0.29 |
| Lawigan | -15.16 | -0.24 | 0.00 | 0.00 |

Table 8 shows the maximum and minimum erosion and accretion rate. Barangay Lucatan has a maximum and minimum erosion rate of -7.71 and -0.29 m/yr, respectively. Barangay Tomoaong has a maximum and minimum erosion rate of -8.93 and -0.14 m/yr, respectively, and maximum and minimum accretion rates of +4.49 and +1.51 m/yr, respectively. Barangay Tagabakid has a maximum and minimum erosion rate of -3.27 and -0.08 m/yr, respectively, and maximum and minimum accretion rates of +0.29 and +0.11 m/yr, respectively. Barangay Mayo has a maximum and minimum erosion rate of -3.84 and -0.53 m/yr, respectively, and a maximum and minimum accretion rate of +3.15 m/yr. Barangay Don Enrique Lopez has a maximum and minimum erosion rate of -6.04 and -0.56 m/yr, respectively. Barangay Dahican has a maximum and minimum erosion rate of -23.60 and -1.88 m/yr, respectively, and maximum and minimum accretion rates of +2.25 and +2.02 m/yr, respectively. Barangay Bobon has a maximum and minimum erosion rate of -27.15 and -7.83 m/yr, respectively. Barangay Tamisan has a maximum and minimum erosion rate of -13.54 and -0.40 m/yr, respectively, and a maximum and minimum accretion rate of +0.29 m/yr. Barangay Lawigan has a maximum and minimum erosion rate of -15.16 and -0.24 m/yr, respectively.

**Table 9.** Shoreline length in km for 2013, 2023, 2063, and 2100.

| Year | 2013 | 2023 | 2063 | 2100 |
|---|---|---|---|---|
| Shoreline length (km) | 47.294 | 47.331 | 49.022 | 54.662 |

Table 9 shows the shoreline length in 2013 and 2023 and the predicted length in 2063 and 2100 using the generated data of shoreline shift rates using DSAS software.

**Table 10.** Shoreline erosion area in km$^2$ (2013, 2023, 2063, and 2100).

| Area | 2023 | 2063 | 2100 |
|---|---|---|---|
| Mayo Bay | 2.968 | 11.060 | 9.800 |

Table 10 shows the shoreline erosion area in square kilometers in 2023 and the predicted erosion area in 2063 and 2100.

**Table 11.** Shoreline accretion area in km$^2$ (2013, 2023, 2063, and 2100).

| Area | 2023 | 2063 | 2100 |
|---|---|---|---|
| Mayo Bay | 0.020 | 0.064 | 0.060 |


DOI: https://doi.org/10.59120/drj.v15i4.269

Table 11 shows the shoreline accretion area in square kilometers in 2023 and the predicted accretion area in 2063 and 2100. Figure 5 shows the length of the shoreline along Mayo Bay in 2013 and 2023 and the predicted shoreline length in 2063 and 2100. Figure 6 shows the extent of erosion and accretion in 2023 and the predicted erosion and accretion coverage in 2063 and 2100.

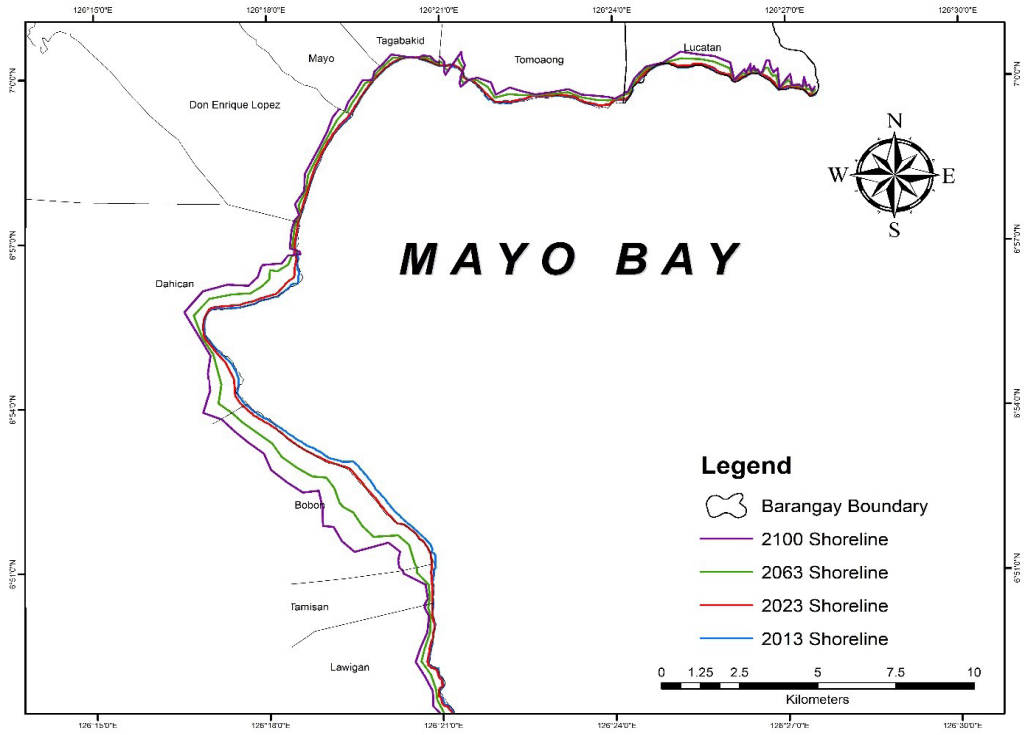


**Figure 5.** Shoreline length (2013, 2023, 2063, and 2100).

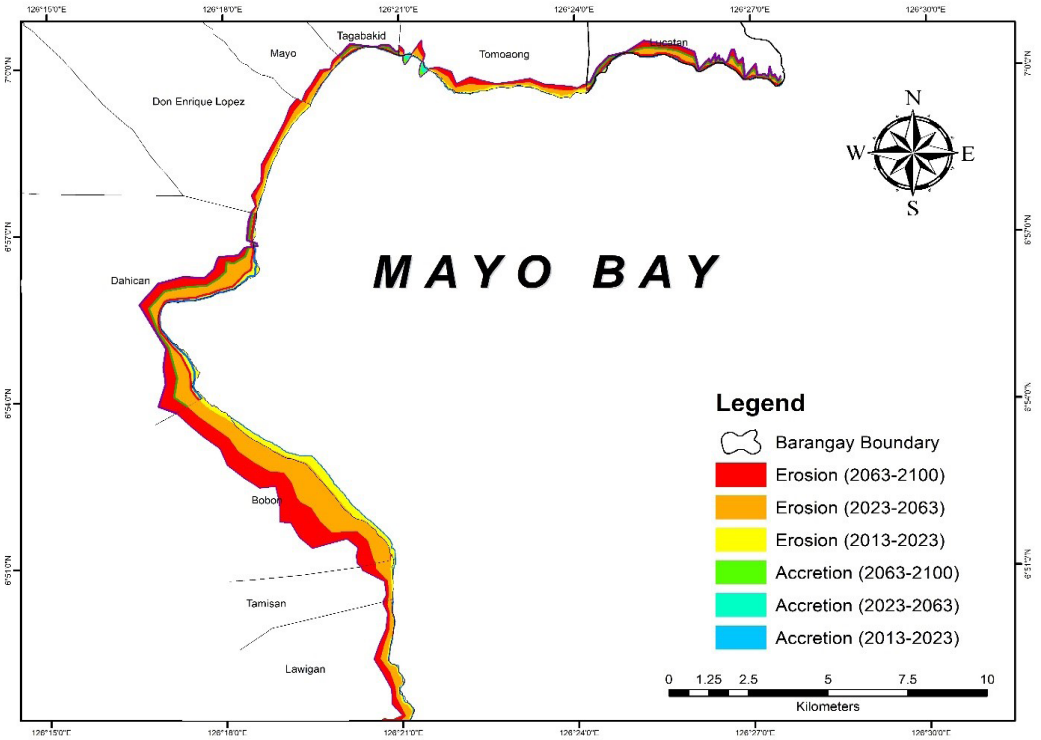


**Figure 6.** Shoreline erosion-accretion (2023, 2063, and 2100).

**Table 12.** Shoreline length (km) for 2013, 2023, 2063, and 2100 per barangay.

| Barangay | Shoreline length (km) | | | |
|---|---|---|---|---|
| | 2013 | 2023 | 2063 | 2100 |
| Lucatan | 7.478 | 7.731 | 8.759 | 10.881 |
| Tomoaong | 7.010 | 6.732 | 7.273 | 8.455 |
| Tagabakid | 1.994 | 1.955 | 2.020 | 2.171 |
| Mayo | 1.920 | 1.866 | 1.920 | 2.042 |
| Don Enrique Lopez | 4.087 | 4.110 | 4.111 | 4.232 |
| Dahican | 8.887 | 8.586 | 9.189 | 10.216 |
| Bobon | 8.379 | 8.453 | 8.543 | 9.105 |
| Tamisan | 1.324 | 1.375 | 1.392 | 1.627 |
| Lawigan | 6.215 | 6.523 | 5.815 | 5.933 |

Table 12 shows shoreline length in kilometers per barangay for 2013, 2023, 2063, and 2100.

**Table 13.** Shoreline erosion area (km$^2$) for 2013-2023, 2023-2063, and 2063-2100.

| Barangay | Erosion area (sq. km) | | |
|---|---|---|---|
| | 2013-2023 | 2023-2063 | 2063-2100 |
| Lucatan | 0.224 | 0.798 | 0.751 |
| Tomoaong | 0.181 | 0.664 | 0.602 |
| Tagabakid | 0.033 | 0.114 | 0.110 |
| Mayo | 0.043 | 0.196 | 0.183 |
| Don Enrique Lopez | 0.119 | 0.404 | 0.418 |
| Dahican | 0.723 | 2.488 | 2.220 |
| Bobon | 1.338 | 5.130 | 4.437 |
| Tamisan | 0.070 | 0.279 | 0.230 |
| Lawigan | 0.237 | 0.987 | 0.849 |

Table 13 shows the shoreline erosion area in square kilometers per barangay for 2013-2023, 2023-2063, and 2063-2100.

**Table 14.** Shoreline accretion area (km$^2$) for 2013-2023, 2023-2063, and 2063-2100.

| Barangay | Accretion area (sq. km) | | |
|---|---|---|---|
| | 2013-2023 | 2023-2063 | 2063-2100 |
| Lucatan | 0.000 | 0.000 | 0.000 |
| Tomoaong | 0.011 | 0.053 | 0.050 |
| Tagabakid | 0.001 | 0.001 | 0.001 |
| Mayo | 0.004 | 0.000 | 0.000 |
| Don Enrique Lopez | 0.000 | 0.000 | 0.000 |
| Dahican | 0.004 | 0.010 | 0.009 |
| Bobon | 0.000 | 0.000 | 0.000 |
| Tamisan | 0.000 | 0.000 | 0.000 |
| Lawigan | 0.000 | 0.000 | 0.000 |

Table 14 shows the shoreline accretion area in square kilometers per barangay for 2013-2023, 2023-2063, and 2063-2100. Figure 7 shows the erosion-accretion map per barangay.


DOI: https://doi.org/10.59120/drj.v15i4.269

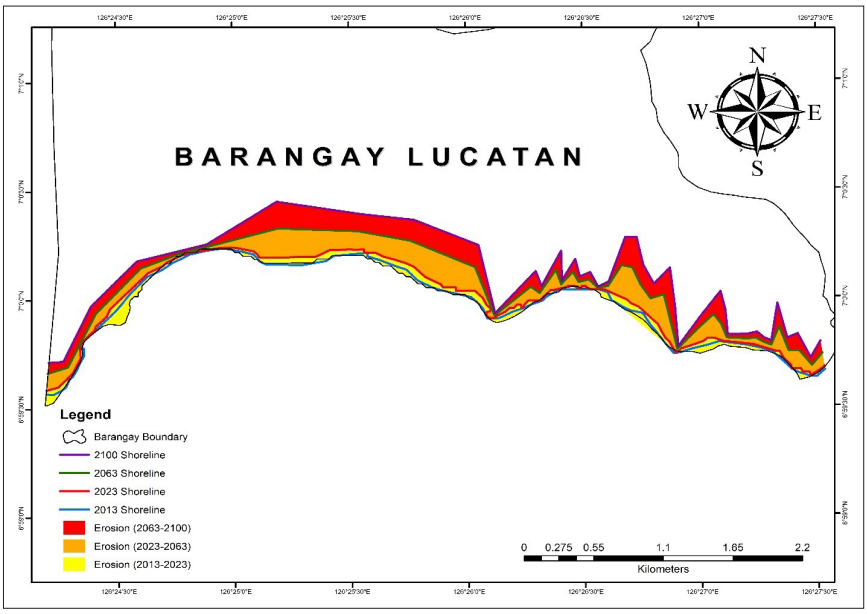
BARANGAY LUCATAN
N
W
E
S
Legend
Barangay Boundary
2100 Shoreline
2063 Shoreline
2023 Shoreline
2013 Shoreline
Erosion (2063-2100)
Erosion (2023-2063)
Erosion (2013-2023)
0 0.275 0.55 1.1 1.65 2.2
Kilometers

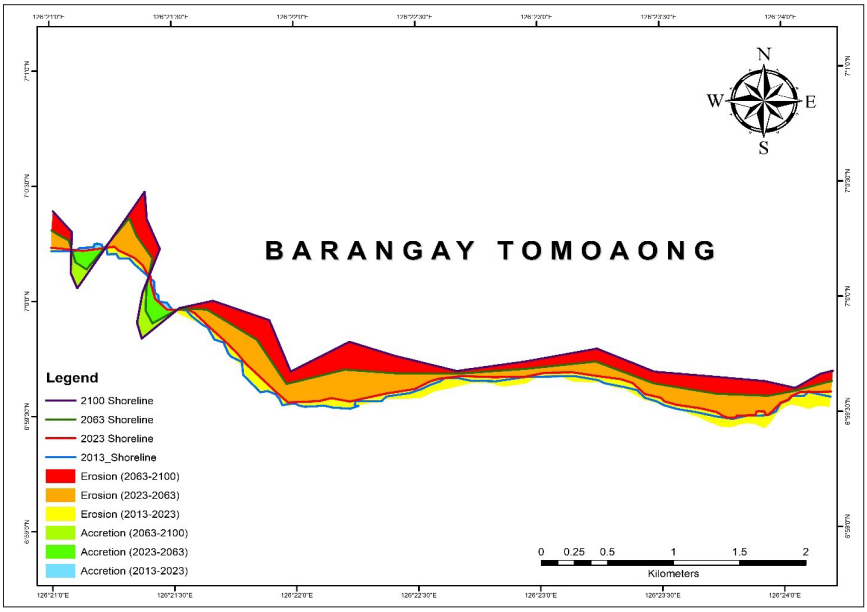
BARANGAY TOMOAONG
N
W
E
S
Legend
2100 Shoreline
2063 Shoreline
2023 Shoreline
2013_Shoreline
Erosion (2063-2100)
Erosion (2023-2063)
Erosion (2013-2023)
Accretion (2063-2100)
Accretion (2023-2063)
Accretion (2013-2023)
0 0.25 0.5 1 1.5 2
Kilometers

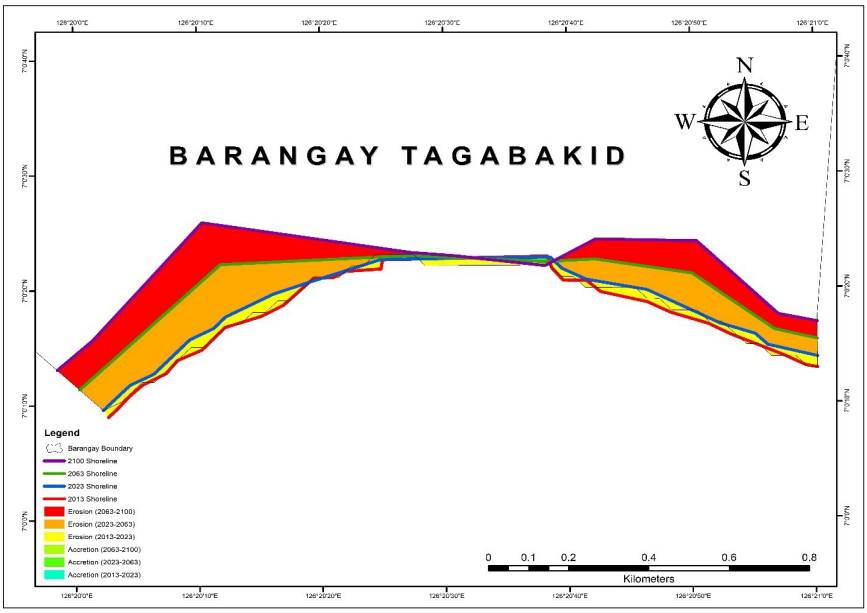
BARANGAY TAGABAKID
N
W
E
S
Legend
Barangay Boundary
2100 Shoreline
2063 Shoreline
2023 Shoreline
2013 Shoreline
Erosion (2063-2100)
Erosion (2023-2063)
Erosion (2013-2023)
Accretion (2063-2100)
Accretion (2023-2063)
Accretion (2013-2023)
0 0.1 0.2 0.4 0.6 0.8
Kilometers

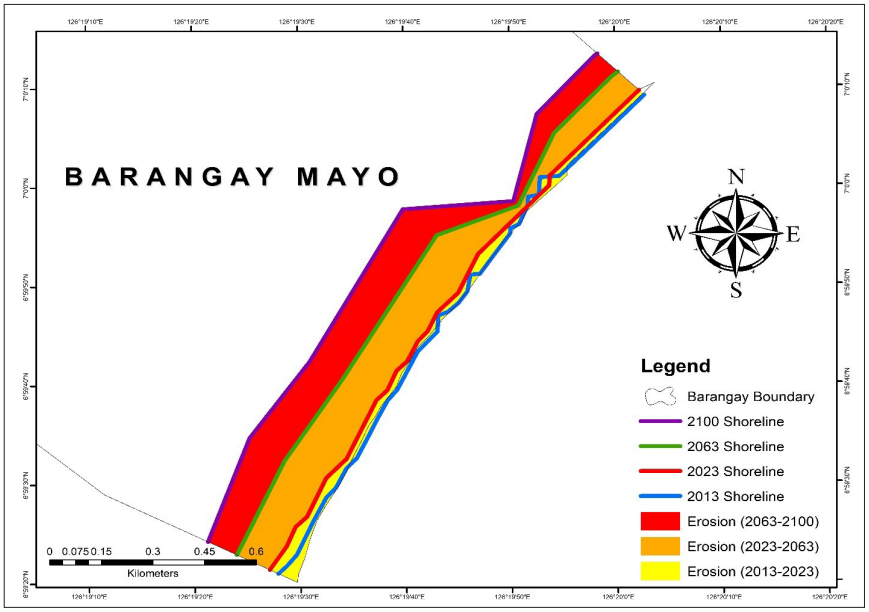


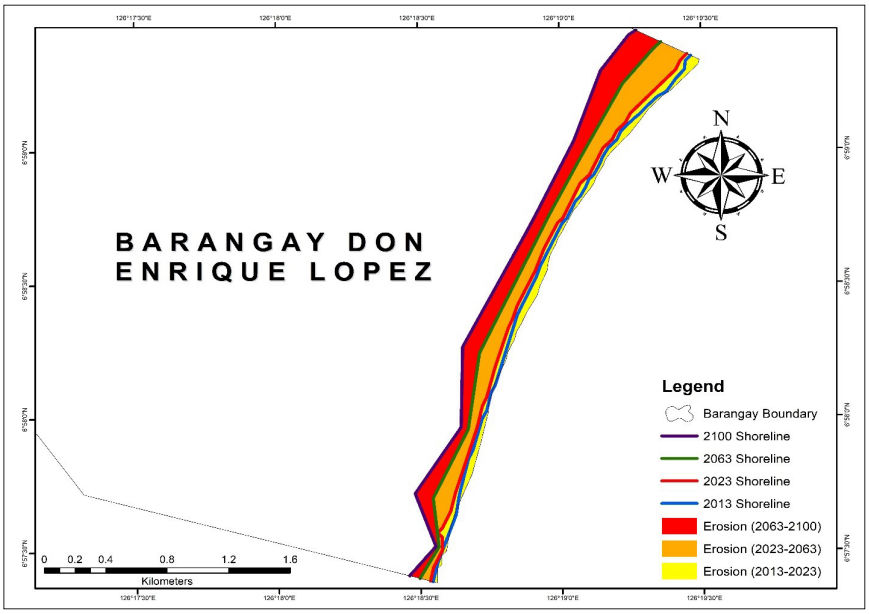


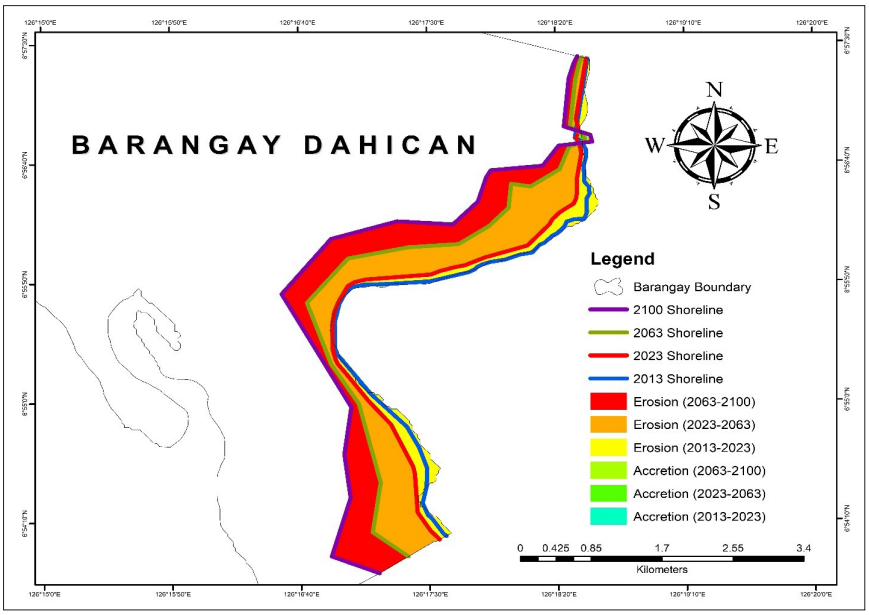


 DOI: https://doi.org/10.59120/drj.v15i4.269

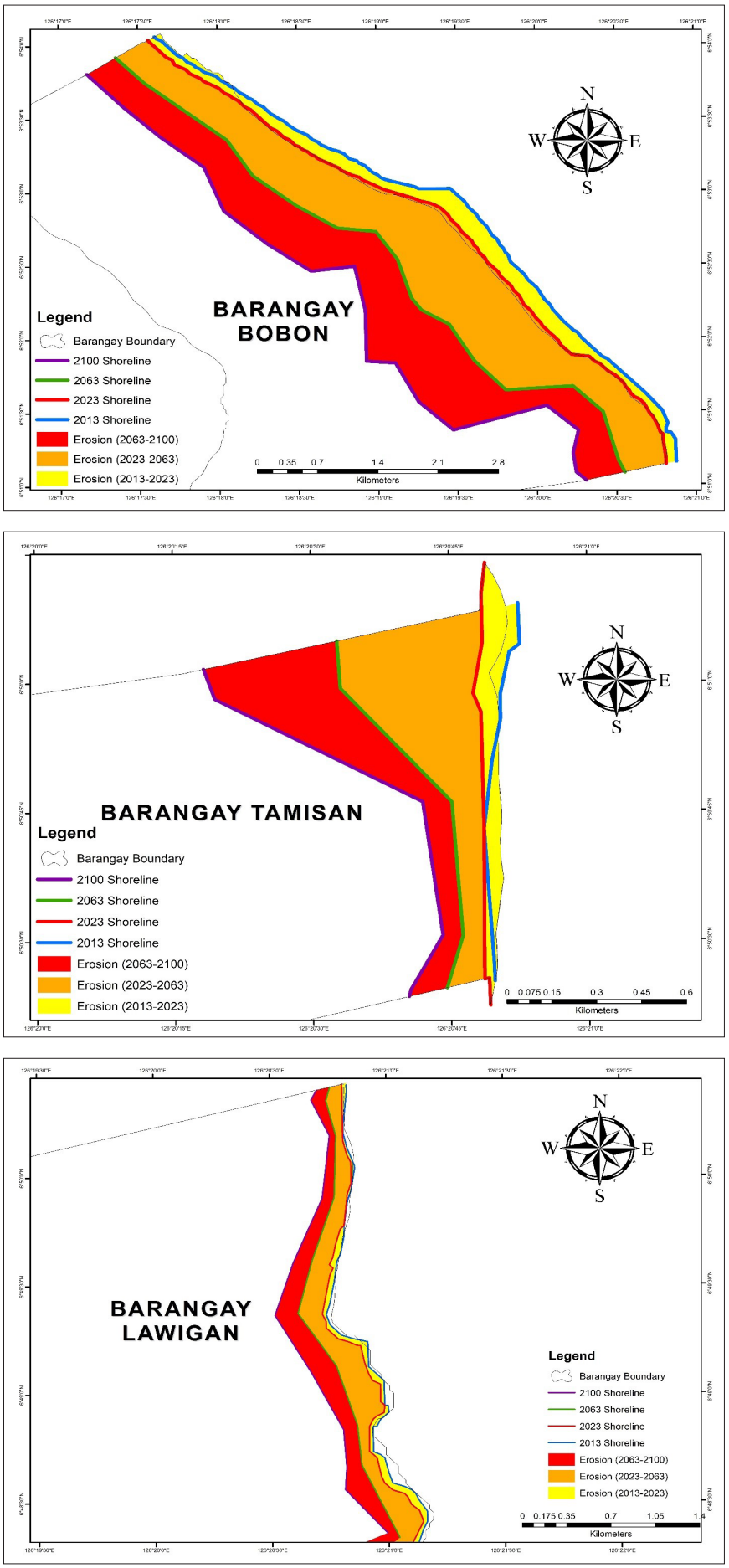


**Figure 7.** Barangay Erosion-Accretion Map.

## DISCUSSIONS

### GIS and RS in shoreline shift

GIS and RS technology have been acknowledged as a leading means for calculating shoreline changes on the temporal scale (Nayak, 2002; Zuzek et al., 2003; Thieler et al., 2009; Kankara et al., 2015). GIS is a helpful tool in mitigating the impacts of a disaster leading to the reduction of a residents' vulnerability to hazards (Masancay et al., 2024). The integration of GIS and RS is beneficial for the management of the coastal zones (Mujabar and Chandrasekar, 2013; Bayram et al., 2013; Goksel et al., 2020) and also effective in the development of any coastal area action plans (Goksel et al., 2020). (Ahmed et al., 2018) investigates the dynamic nature and management aspects of land in the coastal areas of Bangladesh using GIS and RS techniques. Nandi et al. (2026) conducted a case study about coastal shifting and its prediction using GIS and RS techniques on Sagar Island, West Bengal. A survey by Elnabwy et al. (2020) proves that shoreline monitoring can be successfully conducted using only GIS and RS without including the shoreline irregularities attributed to coastal morphological features and climate variables in the analysis. Similar to the study conducted on shoreline shifts in Mayo Bay, which integrates GIS and RS for analysis, this research shows successful detection of shifts and prediction.

### Related shoreline shift studies

Eastern asian region

In 2020, Chu et al. monitored the long-term shoreline dynamics in Hangzhou Bay, China, from 2010 to 2020. The study results show a shoreline movement of 5 km or equivalent to 900 $km^2$. Qiao et al., in the year 2018, conducted a spatiotemporal shoreline change analysis study in Shanghai, China for 1960-to-2015-year interval. The findings of the study suggested a 988 $km^2$ total area shifting. Ciritci and Türk conduct a study on automatic detection of shoreline change in Go¨ksu Delta, Turkey in year 2019. They stress out a severe coastal erosion with an average rate of -30.64 meter per year from year 1984 to 2011 attributes to both natural and human activities particularly the construction of dams and dredging of sand along the area. In 2019, Kale and Acarli conduct a shoreline change monitoring along the coasts of Atikhisar Reservoir, Canakkale, Turkey. The findings of the study show an increase in shoreline total length from 18.8 km in 1995 to 23.1 km in 2014.

Western asian region

Yadav et al. conduct shoreline analysis in 2021 along Rabindranath Tagore beach and Devabagh beach in Karnataka coast, India. It results to an average shoreline change rate of −7.54 meter per year in Devabagh beach and an average shoreline change rate of 0.004 meter per year in Rabindranath Tagore beach from 2013 to 2017. In 2017, Thakur et al. study shoreline change detection in Bakkhali Coastal Region, West Bengal, India for 1990-to-2016-year interval. The results show an increase in human settlement by 77.7% and increase in aquaculture area by 69.75%.

African region

In 2015, Louati et al. assess the change in shoreline Medjerda delta coast, Tunisia from 1972 to 2013 resulting to a severe erosion by -42.6 meter per year. Dadson et al. analyzed the change in shorelines of Cape Coast-Sekondi Coast, Ghana, in 2016, resulting in a long-term erosion change of -1.44 meters per year from 1972 to 2005. An assessment in the shoreline of Watamuarea, Kenya by Alemayehu et al in 2015 resulting to an approximate of about 69% of the beach front from 1969 to 2010.

### Shoreline delineation using satellite imagery data

Shoreline change is a dynamic process (Mills et al., 2005; Qiao et al., 2018) and has become a concern for coastal managers as 60% of the world's population is situated in coastal areas (Boye, 2015). Qiao et al.


DOI: https://doi.org/10.59120/drj.v15i4.269

(2018) strongly stressed that low-lying and vulnerable coastal zones all over the world are vulnerable to possible effects of alterations in shorelines, which is why a long time series of shoreline change data will be of remedy in knowing how shorelines respond to anthropogenic activities and natural events and contribute to future protection of coasts and sustainable development. Boak and Turner (2005), Alemayehu et al. (2015), Srivastava et al. (2005), and Boye (2015) pointed out that shoreline change can be used as a good indicator for possible coastal erosion or coastal accretion. Coastal erosion is the result of the occurrence of shoreline change (Zhang et al., 2004; Boye, 2015). Shoreline change can be illustrated in full detail with the use of spatial data satellite imagery containing high resolution, and with the aid of the satellite temporal resolution, changes can be detected easily (Li and Ma, 2003; Natih et al., 2020). Calculating the rate of change in shorelines and comprehending the processes causing change in shorelines is vital to achieving effective coastal management (Alemayehu et al., 2015). According to Qiao et al. (2018), shorelines' response to anthropogenic activities and natural phenomena will be understood clearly by exploring what causes shoreline change and spatiotemporal dynamic analysis. Causes of shoreline shift are classified into two (2): natural-induced and human-induced activities (Yadav et al., 2017). Natural-induced causes include the processes of coastal erosion, accretion, sea level rise, wave energy, sedimentation, and wind patterns. Yadav et al. (2017) further emphasized that natural-induced causes are the primary causes of shoreline shift. Human-induced activities include Human influence on natural sediment transportation, Beach sediment blockage, and Sediment mining along the coast (Boye, 2015). A combination of satellite-based GIS and RS is used to analyze and extract shorelines. The results of this study proved the statements of Ruiz et al. (2007), Ahmed et al. (2018), and Natih et al. (2020) that using Landsat satellite images is suitable for spatial dynamics monitoring of shorelines. Compared to other techniques, the advantage of using satellite images is their efficiency in considering the large spatial subject area and repeat data collection. There is a lot of shoreline shift detection research that utilizes Landsat imagery (Xu, 2018; Bishop-Taylor et al., 2021; Elnabwy et al., 2020). All of these studies have resulted in a successful analysis of shoreline shifts with the use of Landsat satellite imagery.

**Assessing the accuracy of maps**

The shoreline's accuracy significantly affects the findings of the analyses conducted in shoreline shift analyses (Ciritci & Turk, 2019). The computed kappa statistics of the 2013 and 2023 satellite images are 0.85 and 0.87, respectively, based on the error matrix shown in Table 2. The value was attained using the equation for the kappa statistics formula shown in Chapter 3. According to Rwanga and Ndambuki (2017), the generated map is almost perfect since the kappa value is between 0.81 and 1. The computed overall accuracy of the satellite images is 89.00%. This also suggests that the generated map is good since it is greater than the kappa value. Since both satellite images obtained more than 0.85 or 85% kappa statistics, there is no need for image reclassification since the desired accurate kappa value is attained. The computed RMSE is 0.05, which is based on Table 4. The RMSE value is obtained using the formula shown in Chapter 3. This suggests that the model or the generated maps have good prediction accuracy according to the RMSE ranges in Table 1 for models' performance by Oke et al. (2020) since the RMSE value is between 0.009 and 0.09.

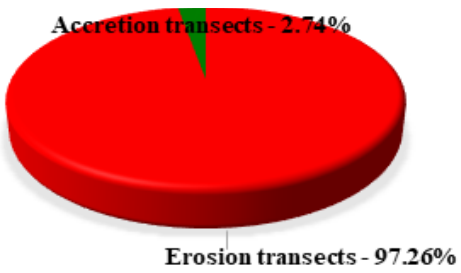


**Figure 8.** Pie chart for erosion-accretion transects.

Figure 8 shows a pie chart illustrating that 97.26% of all the transects are erosion. This suggests that most of the shorelines along Mayo Bay are experiencing shoreline erosion. All portions of the shorelines of barangay Lucatan, Don Enrique Lopez, Bobon, and Lawigan are eroding. Barangay Dahican and Bobon have the highest number of erosion transects, with 92 and 86, respectively, while barangay Tagabakid has the least number of erosion transects, with 13. Barangay Tomoaong has the highest accretion transects with 6.

**Short-term shoreline analysis**

Shoreline shift analysis from 2013 to 2023 serves as the short-term shoreline analysis for this study. Using Table 8 as a reference, it can be observed that the shoreline length in Mayo Bay increased by 0.08% from 2013 to 2023. This suggests that there has been an expansion of the shoreline along Mayo Bay over the years. The erosion area along the shoreline is 2.968 $km^2$. The accretion area along the shoreline is 0.020 $km^2$. Barangay Lucatan, Don Enrique Lopez, Bobon, and Tamisan show an increasing shoreline length. Barangay Lucatan shows the highest increase in shoreline, with an approximate 3.403 km increase. Barangay Bobon, Tamisan, and Don Enrique Lopez show a slight increase in shoreline by 0.726 km, 0.303 km, and 0.145 km, respectively. Barangay Dahican, Tomoaong, Tagabakid, and Mayo decreased in shoreline length from 2013 to 2023. Barangay Lawigan shows a significant increase in shoreline length. It can be observed that all the shorelines per barangay increased except for barangay Lawigan.

**Long-term shoreline analysis**

Shoreline shift analysis after 50 years and at the end of the century is this study's long-term shoreline analysis. The study uses DSAS software to analyze the rate of shifts along the shorelines. DSAS can provide the capability for a systematic and detailed shoreline change rate calculation (Mutaqin, 2017; Arjasakusuma et al., 2021). The EPR method was used because it is the most commonly used method for determining the rate of shift and predicting the future position of the shoreline. It is widely used, especially by coastal land managers and planners, and has become popular due to its robustness and simplicity (Li et al., 2001; Nandi et al., 2016). Moreover, Nandi et al. (2016) also point out that the EPR method is computed using the latest position and a baseline. Any information relevant to the shoreline, such as tidal information, sea current data, sediment supply, sea wave, etc., is not required for analysis because it is only anchored on the historical and recent shoreline map. The total rate of change on shoreline distance is divided by the difference in the elapsed time. It only solves shoreline change rates with two (2) different dates and is calculated for various combinations for more than two shorelines (Ciritci & Türk, 2019). The shoreline is predicted to increase by 3.57% in 2063 and by 11.51% at the end of the century. The data clearly shows a consistent increase in the length of the shoreline over time by 15.58% from 2013 (47.294 km) to 2100 (54.662 km). This suggests that there has been an expansion of the shoreline along Mayo Bay over the years. The erosion area is predicted to increase by 272.64% (11.056 $km^2$) in 2063 and decrease by 11.39% (9.800 $km^2$) in 2100. The accretion area is predicted to increase by 220% (0.064 $km^2$) in 2063 and decrease by 6.67% (0.060 $km^2$) in year 2100. The data shows a decrease from the year 2063 to 2100. Barangay Dahican, Tomoaong, Tagabakid, and Mayo increased in shoreline length from 2063 to 2100. Barangay Lawigan decreased in 2063 and increased again in 2100. Table 12 shows all barangays having an increasing trend in erosion area from 2023 to 2063 and then decreased in 2100. Barangay Bobon has the highest increase in erosion area from 2023 to 2063 (3.793 $km^2$), followed by barangay Dahican with a 1.765 $km^2$ increase and barangay Lawigan with 0.750 $km^2$. The rest of the barangays have a slight increase in erosion area. Barangay Tagabakid has the least increase in erosion area from 2023 to 2063 with 0.081 $km^2$. Barangay Bobon has the highest decrease in erosion area from 2023 to 2063 (0.693 $km^2$), followed by barangay


DOI: https://doi.org/10.59120/drj.v15i4.269

Dahican with 0.268 km$^2$ decrease and barangay Lawigan with 0.138 km$^2$. The rest of the barangays have a slight decrease in erosion area. Barangay Tagabakid had the least decrease in erosion area from 2023 to 2063, with 0.004 km$^2$. Table 12 shows barangays Lucatan, Don Enrique Lopez, Bobon, Tamisan, and Lawigan having no accretion areas. Barangay Tomoaong has increased accretion area from 2023 to 2063 by 0.024 km$^2$ and a decrease of 0.003 km$^2$ in 2100. Barangay Mayo decreased in accretion area by 0.004 km$^2$ from 2023 to 2063. Barangay Dahican increased accretion area by 0.006 km$^2$ and decreased by 0.001 km$^2$ in 2100. Barangay Tagabakid has a consistent accretion area of 0.001 km$^2$. Arjasakusuma (2021) suggests that coastal defense mechanisms anchored by integrated coastal management be imposed in coastal erosion areas to reduce the socioeconomic impact.

## CONCLUSIONS

The study results show that 97.26% of all transects are erosion. This means that most of the shorelines along Mayo Bay are experiencing shoreline erosion. The shoreline slightly increased by 0.08% from 2013 to 2023 and is predicted to increase by 3.57% in 2063 and 11.51% by 2100. The shoreline will increase by 15.58% by the end of the century. Barangay Lucatan shows the highest increase in shoreline length with approximately 3.403 km over a decade, equivalent to a 340.30 m/yr increase rate from 2013 to 2023. All barangay shorelines are increasing in size except for barangay Lawigan.

There is an increase in the area along the shoreline caused by shoreline erosion. The erosion area is expected to increase by 272.64% in 2062 and decrease by 11.39% in 2100. All barangays have an increasing trend in erosion areas from 2023 to 2063 and a decrease in 2100. Barangay Bobon and Dahican currently have the highest erosion area from 2013 to 2023 with 1.338 km$^2$ and 0.723 km$^2$, respectively, and is expected to increase by the end of the century by 4.437 km$^2$ and 2.220 km$^2$, respectively, while the rest of the barangays are experiencing a slight increase. Barangay Tagabakid has the least shoreline erosion area. Barangay Bobon has the highest mean erosion rate of -16.42 m/yr. Barangay Bobon and Dahican have a maximum erosion rate of -27.15 m/yr and 23.60 m/yr, respectively. Most areas are not experiencing accretion, particularly barangay Lucatan, Don Enrique Lopez, Bobon, Tamisan, and Lawigan. Barangay Mayo and Don Enrique Lopez have the highest accretion rate of +0.004 km$^2$. The maximum accretion rate of +4.49 m/yr is in barangay Tomoaong.

The future position of shorelines in 2063 and 2100 is presented in Figure 5, which shows that most shorelines are eroding. If the erosion rate continues at today's speed, coastal communities residing along the shorelines of barangay Bobon and Dahican will be significantly affected compared to the other coastal barangays. These areas will be experiencing severe shoreline erosion by the end of the century.In addition, the kappa statistics for 2013 and 2015 satellite images are 0.85 and 0.87, respectively. This suggests that the satellite images used are almost perfect since both values are between 0.81 and 1.00 based on the rating criteria of kappa statistics by Rwanga and Ndambuki (2017). The overall accuracy for both satellite images is 89%, which suggests that the satellite images used are good since the overall accuracy is greater than that of the kappa statistics. GPS equipment is used to validate the models generated. This will allow the enhancement of the accuracy of the erosion-accretion maps produced through the provision of precise geographic location data, ensuring that the findings from the observations are mapped reliably. The results of the actual reading of ground control points show that the RMSE is 0.05. This suggests that the generated erosion-accretion maps have a good prediction accuracy based on the RMSE ranges for model performance.

Integrating RS and GIS techniques is an effective tool for studying shoreline shifts. The use of RS and GIS can predict shoreline shifts occurring in Mayo Bay over the last decade, which are used for prediction using the EPR method. This paper will offer the essential information and primary knowledge on shoreline shift using RS and GIS on the shorelines of Mayo Bay, as there is currently a lack of published studies on shoreline shift in Davao Oriental and even the Philippines. The result of this study will aid the coastal managers of Mayo Bay, especially now that they are crafting their integrated coastal management policy along the Bay. It is highly recommended that the areas with the highest shoreline erosion rates identified in this study be prioritized and given attention to implementing suitable shoreline policies that are effective, efficient, and sustainable. This study may serve as a baseline for future shoreline shift research in other coastal regions to allow a broader understanding of the dynamics of shorelines across diverse environmental settings. Specifically, Pujada Bay, the adjacent Bay, will benefit from this study as most of their shoreline policymakers are the same as Mayo Bay. Future research might also consider adding climatological factors or components to their study further to investigate the impact of climate change on shorelines.

## RECOMMENDATIONS

It would be ideal for the shoreline areas along Mayo Bay with higher shoreline erosion to be classified as high-risk zones prone to coastal erosion. These parts of the shoreline will be subjected to constant monitoring by the local authorities. Development in this zone is strictly prohibited. If possible, it would also be ideal for the Mayo Bay to be declared as a protected area same with its adjacent Bay, the Pujada Bay to preserve the physical characteristics of the Bay and ensure a long-term ecological sustainability.

## ACKNOWLEDGEMENT

The researchers would like to express their deepest gratitude and appreciation to all those who made significant contributions to the fulfillment of this study. Thank you for your guidance and assistance throughout the process. This research endeavor would not be possible without your support.

## FUNDING SOURCE

Study was self funded.

## REFERENCES

Ahmed, A., Drake, F., Nawaz, R., and Woulds, C. (2018). Where is the coast? Monitoring coastal land dynamics in Bangladesh: An integrated management approach using GIS and remote sensing techniques. *Ocean and Coastal Management*, 151, 10–24. https://doi.org/10.1016/j.ocecoaman.2017.10.030

Alemayehu, F., Onwonga, R., Mwangi, J. K., and Wasonga, O. (2015). Assessment of Shoreline Changes in the Period 1969-2010 in Watamuarea, Kenya.

Arjasakusuma, S., Kusuma, S. S., Saringatin, S., Wicaksono, P., Mutaqin, B. W., and Rafif, R. (2021). Shoreline dynamics in East Java Province, Indonesia, from 2000 to 2019 using multi-sensor remote sensing data. *Land*, 10(2), 100.

Arkema, K.K., Guannel, G., Verutes, G., Wood, S.A., Guerry, A., Ruckelshaus, M., Kareiva, P., Lacayo, M., Silver, J.M., (2013). Coastal habitats shield people and property from sea-level rise and storms. *Nat. Clim. Change* 3 (10), 913–918. http://dx.doi.org/10.1038/nclimate1944.

Bayram, B., Seker, D. Z., Acar, U., Yuksel, Y., Guner, H. A. A., and Cetin, I. (2013). An integrated approach to temporal monitoring of the shoreline and basin of Terkos Lake. *Journal of Coastal Research*, 29(6), 1427-1435.

Bishop-Taylor, R., Nanson, R., Sagar, S., and Lymburner, L. (2021). Mapping Australia's dynamic coastline at mean sea level using three decades of Landsat imagery. *Remote Sensing of Environment,* 267, 112734.

Boak, E. H., and Turner, I. L. (2005). Shoreline definition and detection: a review. *Journal of coastal research,* 21(4), 688-703.

Boye, C. B. (2015). Causes and Trends in Shoreline Change in the Western Region of Ghana (Doctoral dissertation, Ph. D thesis. University of Ghana, Ghana).

Chu, L., Oloo, F., Sudmanns, M., Tiede, D., Hölbling, D., Blaschke, T., and Teleoaca, I. (2020). Monitoring long-term shoreline dynamics and human activities in the Hangzhou Bay, China, combining daytime and nighttime EO data. *Big Earth Data*, 4(3), 242-264.

Church, J. A., and White, N. J. (2011). Sea-level rise from the late 19th to the early 21st century. *Surveys in geophysics*, 32, 585-602.

Ciritci, D., and Türk, T. (2019). Automatic detection of shoreline change by geographical information system (GIS) and remote sensing in the Göksu Delta, Turkey. *Journal of the Indian Society of Remote Sensing*, 47, 233-243.

Crowell, M., Leatherman, S. P., and Buckley, M. K. (1991). Historical shoreline change: error analysis and mapping accuracy. *Journal of coastal research*, 839-852.

Davidson, M. A., Lewis, R. P., and Turner, I. L. (2010). Forecasting seasonal to multi-year shoreline change. *Coastal Engineering*, 57(6), 620-629.

Dellepiane, S., De Laurentiis, R., and Giordano, F. (2004). Coastline extraction from SAR images and a method for the evaluation of the coastline precision. *Pattern Recognition Letters*, 25(13), 1461-1470.

Elnabwy, M. T., Elbeltagi, E., el Banna, M. M., Elshikh, M. M. Y., Motawa, I., and Kaloop, M. R. (2020). An approach based on landsat images for shoreline monitoring to support integrated coastal management - A case study, ezbet elborg, nile delta, Egypt. *ISPRS International Journal of Geo-Information*, 9(4). https://doi.org/10.3390/ijgi9040199

Fenster MS, Dolan R, Morton RA (2001) Coastal storms and shoreline change: signal or noise? *J Coast Res* 17:714–720

Goksel, C., Senel, G., and Dogru, A. O. (2020). Determination of shoreline change along the Black Sea coast of Istanbul using remote sensing and GIS technology. *Desalin. Water Treat.*, 177, 1.

Jimenez, L., and Inabiogan, M. K. (2019a). A survey of cetaceans found in Mayo Bay, Davao Oriental, Philippines. *Davao Research Journal*, 12(2), 30-39.

Jimenez, L. A., and Inabiogan, M. K. D. (2019b). A survey of marine turtles found in Davao Oriental, Philippines. *Davao Research Journal*, 12(2), 1-1.

Jenness, J., and Wynne, J. J. (2007). Kappa analysis (kappa_stats. avx) extension for ArcView 3. x. *Jenness Enterprises.*

Johnston, A., Slovinsky, P., and Yates, K. L. (2014). Assessing the vulnerability of coastal infrastructure to sea level rise using multi-criteria analysis in Scarborough, Maine (USA). *Ocean & Coastal Management*, 95, 176-188.

Kale, S., and Acarli, D. (2019). Shoreline change monitoring in Atikhisar Reservoir by using remote sensing and geographic information system (GIS). *Fresenius Environmental Bulletin*, 28(5), 4329-4339.

Kankara, R. S., Selvan, S. C., Markose, V. J., Rajan, B., and Arockiaraj, S. (2015). Estimation of long and short term shoreline changes along Andhra Pradesh coast using remote sensing and GIS techniques. *Procedia Engineering*, 116, 855-862.

Landis, J.R. and Koch, G.G. (1977) A One-Way Components of Variance Model for Categorical Data. *Biometrics*, 33, 671-679. https://doi.org/10.2307/2529465

Li R, Liu JK, Felus Y (2001) Spatial modelling and analysis for shoreline change detection and coastal erosion monitoring. *Mar Geod* 24:1–12

Li, R., Di, K., and Ma, R. (2003). 3-D shoreline extraction from IKONOS satellite imagery. *Marine Geodesy*, 26(1-2), 107-115.

Louati, M., Saïdi, H., and Zargouni, F. (2015). Shoreline change assessment using remote sensing and GIS techniques: a case study of the Medjerda delta coast, Tunisia. *Arabian Journal of Geosciences*, 8, 4239-4255.

Lu, D.,and Weng, Q. (2007). A survey of image classification methods and techniques for improving classification performance. *International journal of Remote sensing*, 28(5), 823-870.

Maiti, S., and Bhattacharya, A. K. (2009). Shoreline change analysis and its application to prediction: A remote sensing and statistics based approach. *Marine Geology*, 257(1-4), 11-23.

Masancay, F. D., Comendador, Y. J. F., Dizon, J. A. L., and Jallores, L. P. L. (2024). Geographic information system-based prioritization mapping for urban search and rescue in Poblacion, Davao City. *Davao Research Journal,* 15(3), 111-121.

McFeeters, S.K. (1996) The use of the Normalized Difference Water Index (NDWI) in the delineation of open water features, *International Journal of Remote Sensing*, 17:7, 1425-

Mills, J. P., Buckley, S. J., Mitchell, H. L., Clarke, P. J., and Edwards, S. J. (2005). A geomatics data integration technique for coastal change monitoring. Earth Surface Processes and Landforms: *The Journal of the British Geomorphological Research Group,* 30(6), 651-664.

Mondal, I., Bandyopadhyay, J., and Dhara, S. (2017). Detecting shoreline changing trends using principle component analysis in Sagar Island, West Bengal, India. *Spatial Information Research,* 25, 67-73.

Mujabar, P. S., and Chandrasekar, N. (2013). Shoreline change analysis along the coast between Kanyakumari and Tuticorin of India using remote sensing and GIS. *Arabian Journal of Geosciences*, 6, 647-664.

Mutaqin, B. W. (2017). Shoreline changes analysis in kuwaru coastal area, yogyakarta, Indonesia: An application of the digital shoreline analysis system (DSAS). *International Journal of Sustainable Development and Planning*, 12(7), 1203-1214.

NAMRIA, 2015. Philippine Rivers. National Mapping and Resource Information Authority, OCHA.

Nandi, S., Ghosh, M., Kundu, A., Dutta, D., and Baksi, M. (2016). Shoreline shifting and its prediction using remote sensing and GIS techniques: a case study of Sagar Island, West Bengal (India). *Journal of coastal conservation*, 20, 61-80.

Natih, N. M. N., Pasaribu, R. A., Sangadji, M. S., and Kusumaningrum, E. E. (2020). Study on shoreline changes using Landsat imagery in Sangsit Region, Bali Province. In *IOP Conference Series: Earth and Environmental Science* (Vol. 429, No. 1, p. 012059). IOP Publishing.

Nayak, S. (2002). Use of satellite data in coastal mapping. *Indian Cartographer*, 22(147-157), 1.

Oke, E. O., Adeyi, O., Okolo, B. I., Adeyi, J. A., Ayanyemi, J., Osoh, K. A., and Adegoke, T. S. (2020). Phenolic compound extraction from Nigerian Azadirachta indica leaves: response surface and neuro-fuzzy modelling performance evaluation with Cuckoo search multi-objective optimization. *Results in Engineering*, 8, 100160.

Olmanson, L. G., Kloiber, S. M., Bauer, M. E., & Brezonik, P. L. (2001). Image processing protocol for regional assessments of lake water quality. *Water resources center technical report*, 14.

Pajak, M. J., and Leatherman, S. (2002). The high-water line as shoreline indicator. *Journal of coastal research*, 329-337.

Qiao, G., Mi, H., Wang, W., Tong, X., Li, Z., Li, T., and Hong, Y. (2018). 55-year (1960–2015) spatiotemporal shoreline change analysis using historical DISP and Landsat time series data in Shanghai. *International journal of applied earth observation and geoin formation*, 68, 238-251.

Rahman, A. F., Dragoni, D., and El-Masri, B. (2011). Response of the Sundarbans coastline to sea level rise and decreased sediment flow: A remote sensing assessment. *Remote Sensing of Environment,* 115(12), 3121-3128.

 DOI: https://doi.org/10.59120/drj.v15i4.269

Rasuly, A., Naghdifar, R., and Rasoli, M. (2010). Monitoring of Caspian Sea coastline changes using object-oriented techniques. *Procedia Environmental Sciences*, 2, 416-426.

Ruiz, L. A., Pardo, J. E., Almonacid, J., and Rodríguez, B. (2007, July). Coastline automated detection and multi-resolution evaluation using satellite images. In *Proceedings of the Coastal Zone* (Vol. 7, pp. 22-26).

Rwanga, S. S., and Ndambuki, J. M. (2017). Accuracy assessment of land use/land cover classification using remote sensing and GIS. *International Journal of Geosciences*, 8(04), 611.

Schönau, M. C., Rudnick, D. L., Cerovecki, I., Gopalakrishnan, G., Cornuelle, B. D., McClean, J. L., and Qiu, B. (2015). The Mindanao Current: mean structure and connectivity. *Oceanography*, 28(4), 34-45.

Srivastava, A., Niu, X., Di, K., and Li, R. (2005, March). Shoreline modeling and erosion prediction. In *proceedings of the ASPRS annual conference* (pp. 7-11).

Sryberko, A. (2023). Analysis of the application of the Normalized Difference Water Index (NDWI) in the Odesa Bay Area of the Black Sea. Materials of the MCND Conferences, (03.11. 2023; Sumy, Ukraine), 190-192.

SunStar Davao (2020). 3 bays in Mati among most beautiful bays in the world. SunStar. https://www.sunstar.com.ph/davao/local-news/3-bays-in-mati-among-most-beautiful-bays-in-the-world

Szmytkiewicz, M., Biegowski, J., Kaczmarek, L. M., Okroj, T., Ostrowski, R., Pruszak, Z., and Skaja, M. (2000). Coastline changes nearby harbour structures: comparative analysis of one-line models versus field data. *Coastal Engineering*, 40(2), 119-139.

Thakur, S., Dey, D., Das, P., Ghosh, P., and De, T. (2017). Shoreline change detection using remote sensing in the Bakkhali Coastal Region, West Bengal, India. *Indian J. Geosci*, 71, 611-626.

Thieler, E. R., Himmelstoss, E. A., Zichichi, J. L., and Ergul, A. (2009). The Digital Shoreline Analysis System (DSAS) version 4.0-an ArcGIS extension for calculating shoreline change (No. 2008-1278). US Geological Survey.

USGS, (2024). Landsat 8. https://www.usgs.gov/landsat-missions/landsat-8

Xu, N. (2018). Detecting coastline change with all available landsat data over 1986–2015: A case study for the state of Texas, USA. *Atmosphere*, 9(3), 107.

Yadav, A., Dodamani, B. M., and Dwarakish, G. S. (2021). Shoreline analysis using Landsat-8 satellite image. I*SH Journal of Hydraulic Engineering*, 27(3), 347-355.

Yadav, Arunkumar and Dodamani, Basavanand & Dwarakish, And. (2017). Shoreline Change: A Review.

Zhang, K., Douglas, B. C., and Leatherman, S. P. (2004). Global warming and coastal erosion. *Climatic change*, 64, 41-58.

Zuzek, P. J., Nairn, R. B., and Thieme, S. J. (2003). Spatial and temporal considerations for calculating shoreline change rates in the Great Lakes Basin. *Journal of Coastal Research*, 125-146.